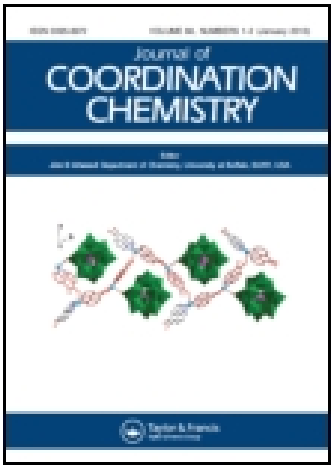

Journal of Coordination Chemistry
Publication details, including instructions for authors and subscription information:
http://www.tandfonline.com/loi/gcoo20

Dinuclear vanadium complexes with rigid phenylpolycarboxylate ligands: synthesis, structure, and catalytic bromination reaction with potential detection of hydrogen peroxide

Rui Zhang[a], Xiao-Xi Zhang[a], Feng-Ying Bai[b], Chen Chen[a], Qing-Lin Guan[a], Ya-Nan Hou[a], Xuan Wang[a] & Yong-Heng Xing[a]

[a] College of Chemistry and Chemical Engineering, Liaoning Normal University, Dalian, PR China

[b] College of Life Science, Liaoning Normal University, Dalian, PR China

Accepted author version posted online: 19 May 2014.Published online: 13 Jun 2014.

To cite this article: Rui Zhang, Xiao-Xi Zhang, Feng-Ying Bai, Chen Chen, Qing-Lin Guan, Ya-Nan Hou, Xuan Wang & Yong-Heng Xing (2014) Dinuclear vanadium complexes with rigid phenylpolycarboxylate ligands: synthesis, structure, and catalytic bromination reaction with potential detection of hydrogen peroxide, Journal of Coordination Chemistry, 67:9, 1613-1628, DOI: 10.1080/00958972.2014.926007

To link to this article: http://dx.doi.org/10.1080/00958972.2014.926007

Journal of Coordination Chemistry, 2014
Vol. 67, No. 9, 1613–1628, http://dx.doi.org/10.1080/00958972.2014.926007

Dinuclear vanadium complexes with rigid phenylpolycarboxylate ligands: synthesis, structure, and catalytic bromination reaction with potential detection of hydrogen peroxide

RUI ZHANG†, XIAO-XI ZHANG†, FENG-YING BAI*‡, CHEN CHEN†, QING-LIN GUAN†, YA-NAN HOU†, XUAN WANG† and YONG-HENG XING**†

†College of Chemistry and Chemical Engineering, Liaoning Normal University, Dalian, PR China
‡College of Life Science, Liaoning Normal University, Dalian, PR China

(*Received 15 August 2013; accepted 11 March 2014*)

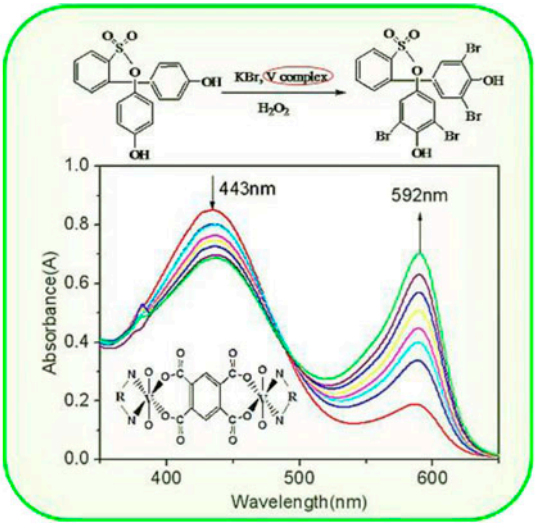

Two oxovanadium complexes, $(VO)_2(2,2'\text{-bipy})_2(bta)(H_2O)_2$ (**1**) and $(VO)_2(1,10\text{-phen})_2(bta)(H_2O)_2$ (**2**) (H_4bta = 1,2,4,5-benzenetetracarboxylic acid, 2,2′-bipy = 2,2-bipyridine and 10-phen = 1,10-phenanthroline), have been synthesized and characterized. The catalytic bromination activity and the practical application of H_2O_2 detection have been studied.

Vanadium complexes $(VO)_2(2,2'\text{-bipy})_2(bta)(H_2O)_2$ (**1**) and $(VO)_2(1,10\text{-phen})_2(bta)(H_2O)_2$ (**2**) (H_4bta = 1,2,4,5-benzenetetracarboxylic acid, 2,2′-bipy = 2,2-bipyridine and 1,10-phen = 1,

*Corresponding authors. Email: baifengying2000@163.com (F.-Y. Bai); xingyongheng@lnnu.edu.cn (Y.-H. Xing)

10-phenanthroline) have been synthesized by the reaction of $V_2(SO_4)_3$, H_4bta, 2,2′-bipy (for **1**) and 1,10-phen (for **2**) by hydrothermal methods. The complexes were characterized by elemental analysis, IR, UV–vis, thermogravimetric analyses, and single-crystal X-ray diffraction. Structural analyses indicate that **1** and **2** are both VO-bta-N-heterocycle system complexes. The central vanadium is coordinated by N_2O_4 donors to form a distorted octahedral geometry. The complexes exhibit catalytic bromination activity in a single-pot reaction with conversion of phenol red to bromophenol blue in a mixed solution of H_2O-DMF at 30 ± 0.5 °C with pH 5.8, indicating that they can be considered as a functional model of vanadium-dependent haloperoxidases. The practical application of H_2O_2 detection has also been studied.

Keywords: Dinuclear oxovanadium complex; 1,2,4,5-Benzenetetracarboxylic acid; Bromination reaction activity; Crystal structure

1. Introduction

Vanadium has received a great deal of attention due to significant roles in biochemical and catalytic properties, such as haloperoxidation, nitrogen fixation, and metalloproteins [1–3]. The metal also has the ability to lower plasma glucose levels, stimulate glucose uptake and glycogen synthesis, and enhance insulin sensitivity [4–6]. Among these properties, vanadium haloperoxidases (V-HPOs) which are found in marine algae are able to accelerate the oxidative halogenation of organic compounds [7–9] in the presence of hydrogen peroxide, organic hydroperoxides, or molecular oxygen [10, 11]. The structure of the active centers of V-HPO reveal the central vanadium to be in a trigonal-bipyramidal environment linked to four oxygens and the axially binding N^{ε} of a histidine residue, which is embedded in the protein molecule, through an extensive hydrogen-bonding network. The active site is considered to consist of oxidovanadium-containing O and N donor ligands [12–16]. In particular, the interaction of simple vanadium species (VO^{2+} and VO^{3+}) with various ON or NN donors having bioactive ligands is of growing interest [17]. In order to explore the relationship between the structure and the catalytic activity of the enzyme mimics, a large number of vanadium complexes have been synthesized. For example, vanadium complexes with poly(pyrazolyl)borate ligands, TpVO(acac) [18] and Tp*VO(Me-acac), etc. [19], peroxidevanadium complexes $VO(O_2)(pzH)(Tp)$ and $VO(O_2)(pz)(pzTp)$, etc. [20], and vanadium complexes with Schiff base ligands, $[VO_2(C_9H_7NO_3)](C_{10}H_{10}N_2)_{0.5}$ and $[VO(C_{10}H_8N_2)(C_9H_7NO_3)]_3$, etc. [21]. The coordination environment of the center vanadium with different –N or –O donors can be proposed as scheme 1, when dinuclear vanadium complexes with N-heterocyclic ligands and rigid polycarboxylates are reported.

Most dinuclear vanadium complexes are bridged by $C_2O_4^{2-}$, such as $(VO_2)_2(\mu_2\text{-}C_2O_4)(C_3H_4N_2)_2$ [22], $V_2(bpz^*eaT)_2(\mu_2\text{-}C_2O_4)(C_2O_4)_2$ [23], etc. Many efforts have been focused to find a new bridged ligand for the synthesis of dinuclear vanadium complexes. As H_4bta is a flexible ligand with four carboxylic groups that can be partially or completely deprotonated, various coordination modes can be realized, while the aromatic ring can stabilize crystal structures via π-stacking interactions. Studies of low valence dinuclear vanadium (III/IV) complexes with H_4bta as ligands were reported. Our group has interest in this family of complexes with some related work having been reported [24]. In order to further study the structure and the function of these vanadium complexes, we synthesized two dinuclear vanadium complexes, $(VO)_2$(2,2′-bipy)$_2$(bta)$(H_2O)_2$ (**1**) and $(VO)_2$(1,10-phen)$_2$(bta)$(H_2O)_2$ (**2**) with H_4bta as ligand, and studied the bromination activity. The detection of c (H_2O_2) by the colorimetric method in the bromination reaction system is reported.

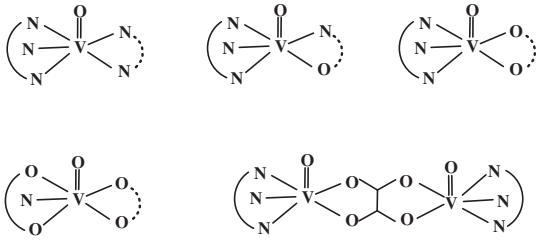

Scheme 1. The coordinated environments of vanadium with different –N or –O ligands.

2. Experimental

2.1. *Materials and methods*

All chemicals used were of analytical grade and used without further purification. Elemental analyses for C, H, and N were carried out on a Perkin Elmer 240C automatic analyzer. Infrared spectra were recorded on a JASCO FT/IR-480 spectrometer with pressed KBr pellets from 200 to 4000 cm^{-1}. UV–vis spectra were recorded on a JASCO V-570 spectrometer (200–1100 nm, in form of solid sample). Thermogravimetric analyses (TG) were performed under air with a heating rate of 10 °C min^{-1} on a Perkin Elmer Diamond TG/DTA.

2.2. *Synthesis of the complexes*

2.2.1. $(VO)_2(2,2'\text{-bipy})_2(bta)(H_2O)_2$ (1). $V_2(SO_4)_3$ (0.25 mM, 0.098 g), 2,2′-bipy (0.25 mM, 0.042 g), and H_4bta (0.25 mM, 0.064 g) were dissolved in methanol–water (3 : 1) mixed solution, stirred for 1–2 h at room temperature, giving a yellow–green solution. Then, the mixture was sealed in a Teflon-lined autoclave and heated at 100 °C for three days, cooled to room temperature and green crystals of **1** were obtained in ca. 52.6% yield based on V(IV). Anal. Calcd for $C_{30}H_{22}O_{12}N_4V_2$: C, 49.16; H, 2.98; N, 7.67. Found: C, 49.23; H, 3.21; N, 7.76. IR (KBr, ν, cm^{-1}): 3060, 1599, 1378, 1487, 1444, 1320, 1164, 1024, 981, 457, 400. UV–vis (λ_{max}, nm): 256, 316, 388, 750.

2.2.2. $(VO)_2(1,10\text{-phen})_2(bta)(H_2O)_2$ (2). The synthesis of **2** was similar to that of **1;** however, 2,2′-bipy was replaced by 1,10-phen (0.25 mM, 0.045 g). Green crystals of **2** were obtained in ca. 63.4% yield based on V(IV). Anal. Calcd for $C_{34}H_{22}O_{12}N_4V_2$: C, 52.32; H, 2.84; N, 7.18. Found: C, 52.41; H, 3.02; N, 7.26. IR (KBr, ν, cm^{-1}): 3059, 1616, 1519, 1485, 1428, 1373, 1343, 1146, 1107, 982, 849, 726, 647, 458, 429, 396. UV–vis (λ_{max}, nm): 262, 304, 356, 444, 780.

2.3. *X-ray single crystal structural determination*

The crystals of **1** and **2** were mounted on a glass fiber for X-ray measurement. Reflection data were collected at room temperature on a Bruker AXS SMART APEX II CCD diffractometer with graphite-monochromated Mo Kα radiation ($\lambda = 0.71073$ Å) and a ω scan mode. All the measured independent reflections ($I > 2\sigma(I)$) were used in the structural analyses, and semi-empirical absorption corrections were applied using SADABS [25]. The structure

Table 1. Crystallographic data and structure refinement for **1**.

Formula	$C_{30}H_{22}N_4O_{12}V_2$
M (g M^{-1})	732.4
Crystal system	Monoclinic
Space group	$P2_1/n$
a (Å)	10.8353(7)
b (Å)	11.8109(8)
c (Å)	12.1040(7)
α (°)	90
β (°)	102.7910(10)
γ (°)	90
V (Å^3)	1510.57(17)
Z	1
D_{Calcd} (Mg m^{-3})	1.610
Crystal size (mm^3)	0.58 × 0.32 × 0.16
F (0 0 0)	744
μ (Mo Kα) (mm^{-1})	0.692
Reflections collected	9319
Independent reflections ($I > 2\sigma(I)$)	3648(2914)
Parameters	214
$\Delta(\rho)$ (e Å^{-3})	0.562 and −0.746
Goodness-of-fit	1.037
R_1[a]	0.0394(0.0538)[b]
wR_2[a]	0.1079(0.1172)[b]

[a]$R_1 = \Sigma||F_o| - |F_c||/\Sigma|F_o|$, $wR_2 = \{\Sigma w(F_o^2 - F_c^2)^2/\Sigma w(F_o^2)^2\}^{1/2}$, $[F_o > 4\sigma(F_o)]$.
[b]Based on all data.

was solved by the direct method using SHELXL-97 [26]. All hydrogens of organic ligand were fixed at calculated positions geometrically and refined using a riding model. Hydrogens of coordination water were located in difference Fourier maps. The non-hydrogen atoms were refined with anisotropic thermal parameters. Crystallographic data and the structure refinements are given in table 1.

2.4. *Measurement of bromination activity in solution*

Brominations were carried out at 30 ± 0.5 °C. Oxidovanadium complex was dissolved in a mixed solution of 25 mL H_2O-DMF (DMF: 2 mL; H_2O: 23 mL). The solutions used for kinetic measurements were maintained at a constant concentration of H^+ (pH 5.8) by the addition of NaH_2PO_4–Na_2HPO_4 buffer solution [27]. Reactions were initiated with the presence of phenol red solution. Five different concentrations of oxidovanadium complex were placed in five cuvettes and then put into the constant temperature water bath. The spectral changes were recorded using a 721 UV–vis spectrophotometer at 5 min intervals, and the resulting data were collected during the reaction.

It was assumed that the rate of this reaction is described by the rate equation: $dc/dt = kc_1^x c_2^y c_3^z$, from which the equation "$\log(dc/dt) = \log k + x\log c_1 + y\log c_2 + z\log c_3$" was obtained, corresponding to "$-\log(dc/dt) = -x\log c_1 - b$ ($b = \log k + y\log c_2 + z\log c_3$)," where k is the reaction rate constant; c_1, c_2, and c_3 are the concentrations of the complex, the KBr, and the phenol red, respectively; while x, y, and z are the corresponding reaction orders. According to Beer–Lambert's law, $A = \varepsilon \cdot d \cdot c$, which is differential, $dA/dt = \varepsilon \cdot d \cdot (dc/dt)$, where A is the measurable absorbance of the resultant; ε is molar absorption coefficient, of which the bromophenol blue is measured as 14,500 M^{-1} cm^{-1} at 592 nm; d is light path length of

sample cell ($d = 1$). When the measurable absorbance data were plotted *versus* reaction time, a line was obtained and the reaction rate of the complexes (dA/dt) was given by the slope of the line. By changing the concentration of the oxovanadium complex in the reaction system, a series of dA/dt data could be obtained. The reaction rate constant (k) could be obtained according to a plot of $-\log(dc/dt)$ *versus* $-\log c_1$ and were fitted using the curve-fitting software in Microsoft Excel by generating least squares fit to a general equation of the form "$y = mx - b$," in which "m" is the reaction order of the oxovanadium complex in this reaction and "b" is the intercept of the line. In the experiment, considering that the reaction orders of KBr and phenol red (y and z) are 1 according to the literature [12, 28]; c_2 and c_3 are 0.4 and 10^{-4} M L^{-1}, respectively. Based on the equation "$b = \log k + y\log c_2 + z\log c_3$," and then the reaction rate constant (k) can be obtained. The bromination of phenol red was monitored by measurement of the absorbance at 592 nm for the reaction solution, taken at specific time points and diluted into the phosphate buffer solution (pH 5.8).

3. Results and discussion

3.1. *Synthesis*

Two vanadium coordination complexes with H_4bta as ligand have been synthesized by hydrothermal methods at 100 °C (scheme 2). Although the complexes have been synthesized in the literature [29], single crystal structure data were not obtained. $V_2(SO_4)_3$ (III) was used in the synthetic process of the complexes, however, the valence state of vanadium has been changed. The reason may be that the higher temperature led to V(III) oxidizing into V(IV) by oxygen in the air. Because the starting material $V_2(SO_4)_3$ (III) is not soluble in common solvents, **1** and **2** could not obtained by conventional synthesis.

3.2. *Spectra properties*

3.2.1. IR spectra. IR spectra of **1** and **2** are shown in figure S1 (see online supplemental material at http://dx.doi.org/10.1080/00958972.2014.926007) and selected data are listed in table 2. The weak peaks observed at 3000–3100 cm^{-1} are attributed to the =C–H stretch [24]. The strong peaks at 1600 cm^{-1} (1599 cm^{-1} for **1** and 1616 cm^{-1} for **2**) and 1380 cm^{-1} (1378 cm^{-1} for **1** and 1373 cm^{-1} for **2**) are attributed to asymmetric and symmetric stretches of C=O group, respectively [30]. Peaks at 1000–1500 cm^{-1} are assigned to stretching vibrations of pyridine [31]. The strong and sharp stretch of V=O are observed in the region of 981–982 cm^{-1} [32] and 457–458 cm^{-1} are due to the V–O stretch, while bands at 396–400 cm^{-1} are assigned to V–N stretch [33]. The infrared spectra of the complexes are consistent with the structural characterization of **1** and **2**.

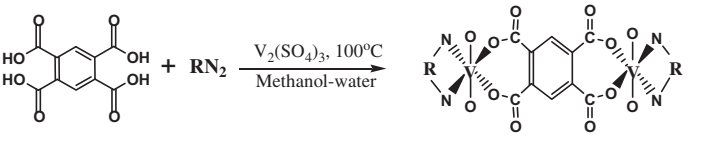

Scheme 2. The synthesis of **1** and **2** (for **1**: RN_2 = 2,2′-bipy; for **2**: RN_2 = 1,10-phen).

Table 2. IR data (cm^{-1}) for **1** and **2**.

Complexes	**1**	**2**
$\nu_{(=C-H)}$	3060	3059
$\nu_{as(COO^-)}$	1599	1616
$\nu_{s(COO^-)}$	1378	1373
Pyridine ring	1487, 1444, 1320, 1164, 1024	1485, 1428, 1343, 1146, 1107
$\nu_{(V=O)}$	981	982
$\nu_{(V-O)}$	457	458
$\nu_{(V-N)}$	400	396

3.2.2. UV–vis absorption spectra. UV–vis absorption spectra of **1** and **2** (Supplementary material) were recorded as solid samples (figure S2). The high-frequency absorptions at 256–262 nm are assigned to π–π^* transitions of the aromatic-like chromophore from 2,2′-bipy, H_4bta and 1,10-phen [34]. Absorptions at 304–444 nm are attributed to LMCT (ligand to metal charge transfer) transition. For vanadyl(IV) complexes, it is generally considered that transitions occur from d_{xy} to (d_{xz}, d_{yz}) (*v1*), d^2_x–d^2_y(*v2*), and d^2_z(*v3*) orbitals with increasing energies. Complexes **1** and **2** exhibit a set of absorptions with maximum wavelength at 750–780 nm, which can be assigned to (ν_1) bands of oxovanadium(IV) [35].

3.3. *Structural description of 1 and 2*

The molecular structure of **1** is depicted in figure 1. Selected bond distances, bond angles, and hydrogen bonds are summarized in table 3.

Structural analysis shows that **1** crystallizes in the monoclinic system with $P2_1/n$ space group. The molecular structure of **1** contains two vanadiums, two terminal oxygens, one H_4bta, two 2,2′-bipy, and two coordinated waters. The binuclear molecule is centrosymmetric, while the coordination environment of the two vanadiums is the same, so we take one for an example. The oxidation state of vanadium is +4, confirmed by Bond-Valence Theory. The vanadium is coordinated by one terminal oxygen (O1), N1 and N2 from 2,2′-bipy, O2 from coordinated water, and two oxygens (O3 and O4) from H_4bta, to form a distorted octahedron. The deviations of O2, O3, O4, and N1 that composed the least-squares plane are 0.0389, −0.0421, 0.0396, and −0.0365 Å, respectively, showing that these atoms are almost on one plane. The V, O1, and N2 from the axial positions lay 0.3205, 1.9120, and −1.9217 Å out of the equatorial plane, indicating that V is toward O1, trans toward N2. The distance of V=O (1.6030(17) Å) is within the range reported for VO^{2+} complexes [23, 33,

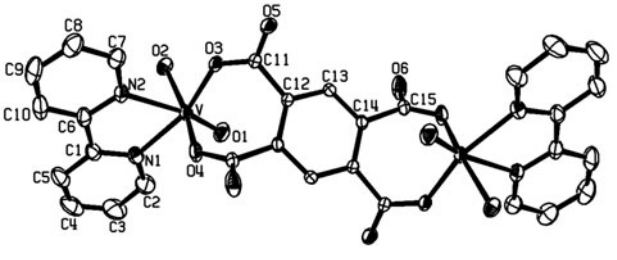

Figure 1. The molecular structure of **1** (hydrogens are omitted for clarity).

Table 3. Selected bond distances (Å), angles (°) and hydrogen bonds (Å) of **1**.

Selected bond lengths (Å) and angles (°)							
V–O1	1.6030(17)	V–O2	2.0507(15)	V–O3	1.9657(15)	V–O4	1.9949(16)
V–N1	2.142(2)	V–N2	2.2619(18)				
O1–V–O3	106.97(8)	O1–V–O4	100.75(9)	O3–V–O4	87.36(7)	O1–V–O2	95.48(8)
O3–V–O2	86.74(6)	O4–V–O2	163.73(7)	O1–V–N1	93.21(8)	O3–V–N1	159.77(8)
O4–V–N1	90.40(7)	O2–V–N1	89.92(7)	O1–V–N2	165.73(8)	O3–V–N2	86.88(7)
O4–V–N2	82.96(7)	O2–V–N2	81.59(7)	N1–V–N2	72.89(8)		

Hydrogen bonds (Å)				
D–H···A	d(D–H)/Å	d(H···A)/Å	d(D···A)/Å	∠D–H···A/°
$O2^{\#2}$–$H2A^{\#2}$···O5	0.9000	1.8354	2.7025	161.03
$C4^{\#1}$–$H4^{\#1}$···O5	0.9300	2.4356	3.3220	159.32
$C9^{\#2}$–$H9^{\#2}$···$O5^{\#3}$	0.9300	2.5838	3.5045	170.57

Note: Symmetry transformation used to generate equivalent atoms: #1: $1-x, -y, -z$; #2: $x, y, -1+z$; #3: $-0.5+x, 0.5-y, 0.5+z$.

36, 47]. The V–O_{water} distance is 2.0507 Å, close to the typical bond lengths for V–OH_2 bond [37]. V–$O_{carboxyl}$ distances are 1.9657 and 1.9949 Å, shorter than that of $[V_2(dipic)_2(H_2bta)(H_2O)_4]\cdot 2H_2O$ (H_2dipic = 2,6-pyridinedicarboxylic acid) [24], which can be explained as the consequence of the different coordinated H_4bta ligand. The bond lengths of V–N are 2.142(2) and 2.2619(18) Å, which are close to reported values [38]. The angles of the O–V–O and O–V–N are 86.74(6)–163.73(7)° and 81.59(7)–165.73(8)°, respectively, and the angle of N–V–N is 72.89(8)°.

There are three kinds of hydrogen bonds (figure 2) in **1**: (i) hydrogen bond between coordinated oxygen and oxygen from the carboxylate of H_4bta, $O2^{\#2}$–$H2A^{\#2}\cdots O5$ (2.7025 Å, 161.03°, #2: x, y, $-1+z$); (ii) hydrogen bond between oxygen from the carboxylate of

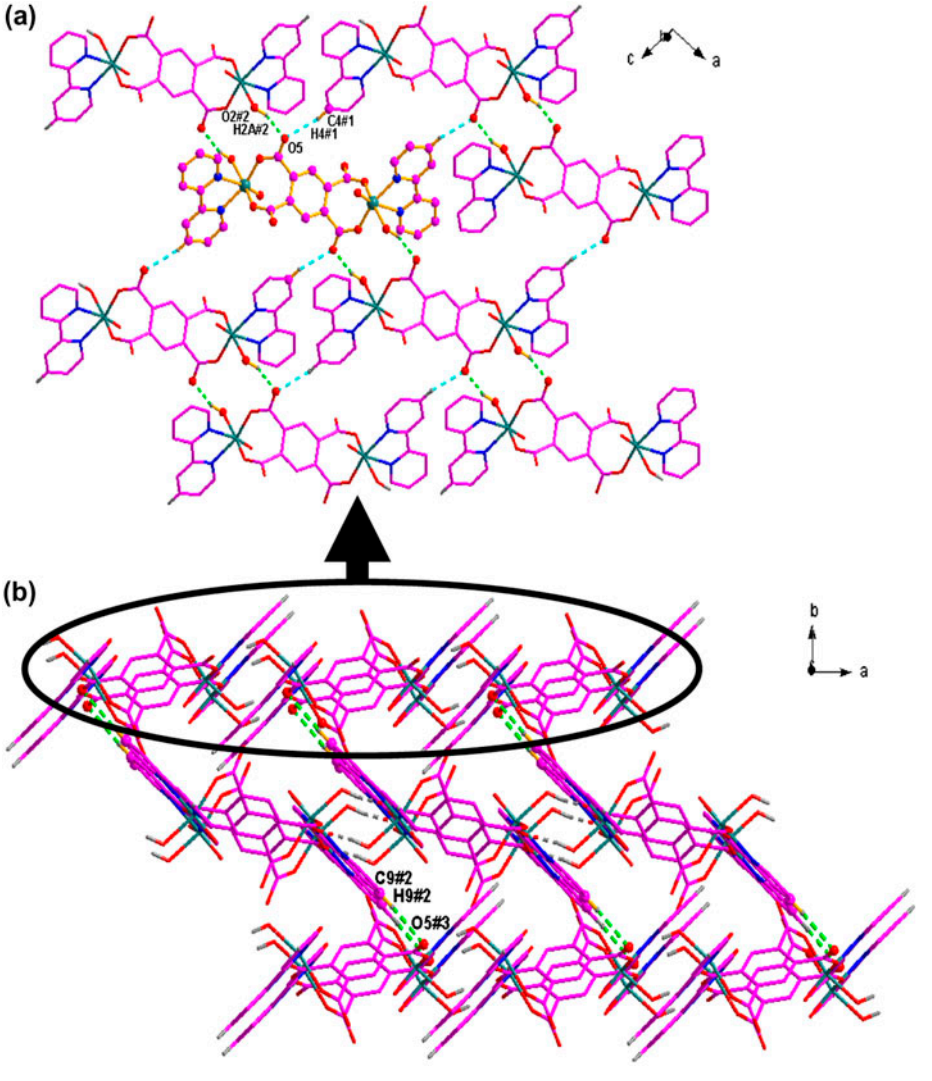

Figure 2. (a) A view of 2-D hydrogen bonding network in **1**; (b) a view of 3-D hydrogen bonding network (all hydrogens except for the hydrogen bonds are omitted for clarity).

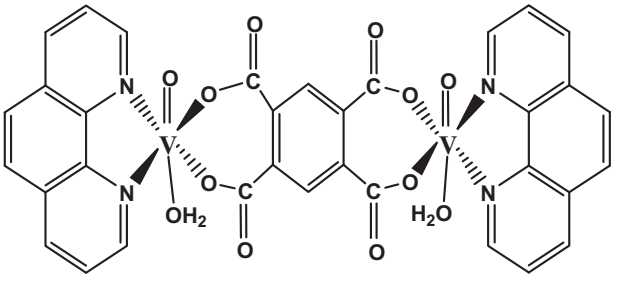

Figure 3. The proposed structure of **2**.

H_4bta and carbon of 2,2′-bipy: $C4^{\#1}$–$H4^{\#1}\cdots O5$ (3.3220 Å, 159.32°, #1: $1-x$, $-y$, $-z$); $C9^{\#2}$–$H9^{\#2}\cdots O5^{\#3}$ (3.5045 Å, 170.57°, #3: $-0.5+x$, $0.5-y$, $0.5+z$). The molecules are connected to a 2-D superamolecular sheet by the hydrogen interactions of $O2^{\#2}$–$H2A^{\#2}\cdots O5$ and $C4^{\#1}$–$H4^{\#1}\cdots O5$; (iii) neighboring sheets are connected to a 3-D network through the hydrogen interactions of $C9^{\#2}$–$H9^{\#2}\cdots O5^{\#3}$.

The structure of **2** is similar to that of **1** (figure 3), confirmed by IR and UV–vis spectroscopy, elemental analyses, and TG. However, its crystal structure data was not obtained because of poor quality of the crystal.

3.4. *Thermal properties*

To examine the thermal stabilities of **1** and **2**, TG was carried out at a heating rate of 10 °C min^{-1} under N_2 from 30 to 1000 °C (figure 4). The TG curve of **1** shows two stages, the first stage occurs from 30 to 576 °C with weight loss of 59.59% (Calcd 59.67%), which is attributed to release of two coordinated waters, two 2,2′-bipy and two coordinated carboxyl. The second stage is observed from 576 to 1000 °C, which is considered from two coordinated carboxyl and the gradual decomposition of the framework of H_4bta. The TG curve of

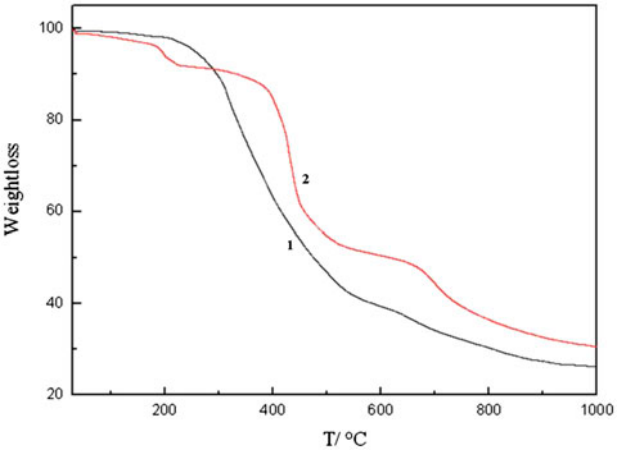

Figure 4. The TG curves for **1**.

2 can be divided into three stages. The initial weight loss of 5% (Calcd 4.62%) from 30 to 197 °C is due to the release of two coordinated waters. The second weight loss of 45.49% (Calcd 46.18%) at 197 to 632 °C is from the release of two 1,10-phen. The last step of decomposition occurred from 632 to 1000 °C, from loss of H_4bta. The final residue corresponds to vanadium oxide and nitride.

3.5. *XRD analysis*

The powder X-ray diffraction data of **1** was obtained and compared with the corresponding simulated single-crystal diffraction data (figure 5). The complex is considered pure owing to agreement of the peak positions. The different intensities may be due to preferred orientation of the powder samples.

3.6. *Functional mimics of the V-HPOs*

3.6.1. Mimicking bromination of the complexes. Oxidovanadium complexes are able to mimic a reaction in which V-HPOs catalyze the bromination of organic substrates in the presence of H_2O_2 and bromide [39, 40]. For example, bromination of trimethoxybenzene [41], benzene, salicylaldehyde, and phenol by VO_2^+ [42], and the bromination of phenol red by $[VO(O_2)H_2O]^+$ and related species [43]. Herein, the bromination activity of **1** and **2** using phenol red as substrate, which is shown by conversion of phenol red to bromophenol blue, has been investigated. The reaction is rapid and stoichiometric, producing the halogenated product by reaction of oxidized halogen species with the organic substrate, and the reactive process is shown in scheme 3.

Addition of the solution of **1** to the standard reaction of bromide in a phosphate buffer with phenol red as a trap for oxidized bromine resulted in color change of the solution from yellow to blue. The electronic absorption showed a decrease in absorbance of the peak at 443 nm from loss of phenol red and an increase of the peak at 592 nm with production of

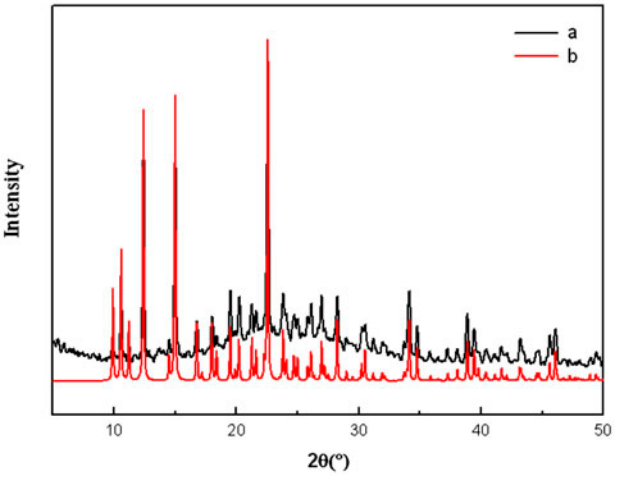

Figure 5. The simulation XRD (a) and experimental XRD (b) spectrum of **1**.

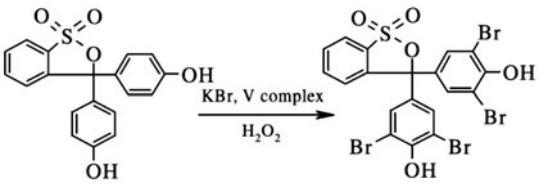

Scheme 3. The reactive process of bromination reaction for the complexes.

bromophenol blue (shown in figure 6), showing that **1** possesses better catalytic activity. The catalytic activity for **2** is similar to that of **1**.

3.6.2. Kinetic studies of bromination. We used **2** to carry out kinetic studies of bromination. A series of dA/dt data were obtained by changing the concentration of the oxovanadium complex, then the plot of $-\log(\mathrm{d}c/\mathrm{d}t)$ *versus* $-\log c$ for **2** was depicted according to the data of figure 7, obtaining a straight line (figure 8) with a slope of 1.018 and an intercept of −2.1331. The former confirms the first-order reaction is dependent on vanadium. Based on the equation "$b = \log k + y\log c_2 + z\log c_3$," the reaction rate constant, k, is determined by the concentrations of KBr and phenol red (c_2 and c_3), the reaction orders of KBr and phenol red (y and z), as well as b. Considering that the reaction orders of KBr and phenol red (y and z) are 1 according to the literature [44]; c_2 and c_3 are known to be 0.4 and $10^{-4}\,\mathrm{M\,L^{-1}}$, respectively, so the reaction rate constant (k) for **2** can be calculated as $0.184 \times 10^3\ (\mathrm{M\,L^{-1}})^{-2}\,\mathrm{s^{-1}}$.

Similar plots for **1** were generated in the same way (figures S3 and S4), and values of the slope and the intercept are 1.0033 and −2.1251, respectively.

The results show that: (i) the reaction orders of the oxidovanadium complexes in bromination reactions are close to **1**, confirming the first-order dependence on vanadium; (ii) the reaction rate constants of the two complexes are close, which is probably due to similarity of their structures.

The halide oxidation catalytic reaction mechanism for the oxovanadium complexes in this work is shown in scheme 4. The peroxidovanadium intermediate $[VO(O_2)N_2]$ was formed

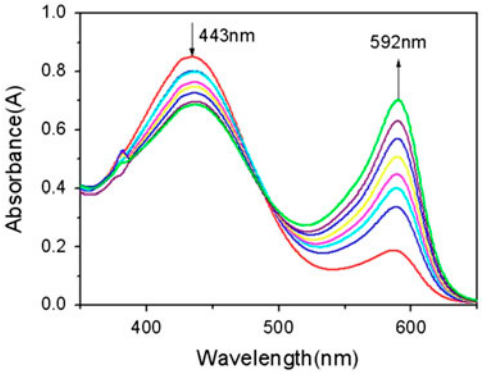

Figure 6. Oxidative bromination of phenol red catalyzed by **1**. Spectral changes at 10 min intervals. The reaction mixture contained phosphate buffer (pH 5.8), KBr ($0.4\,\mathrm{M\,L^{-1}}$), phenol red ($10^{-4}\,\mathrm{M\,L^{-1}}$), and **1** ($0.1\,\mu\mathrm{M\,L^{-1}}$).

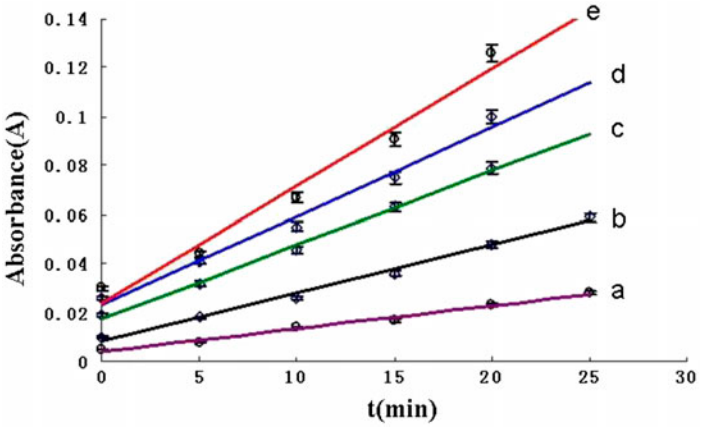

Figure 7. A series of linear calibration plots of the absorbance at 592 nm dependence of time for different concentration of **2**. Condition used: pH 5.8, c(KBr) = 0.4 M L^{-1}, c(H_2O_2) = 1 M L^{-1}, c(phenol red) = 10^{-4} M L^{-1}. c(complex **2**/mM L^{-1}) = a: 1.08×10^{-5}; b: 2.15×10^{-5}; c: 3.23×10^{-5}; d: 4.31×10^{-5}; e: 5.38×10^{-5}. Error bars shown are three standard deviations for three independent measurements.

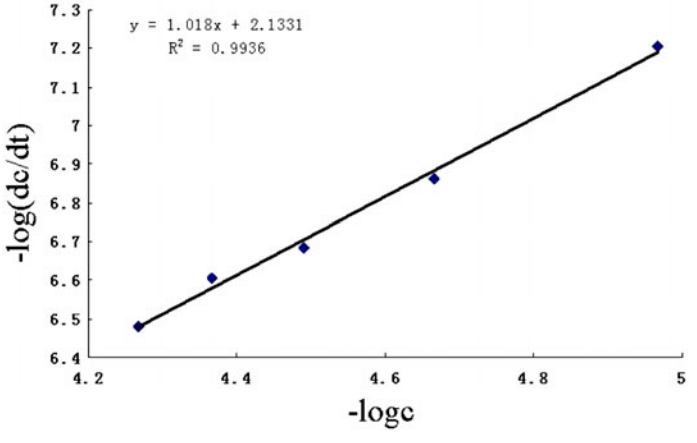

Figure 8. −Log(d*c*/d*t*) dependence of −log*c* for **2** in DMF-H_2O at 30 ± 0.5 °C (*c* is the concentration of **2**).

by action of oxidovanadium complexes with H_2O_2 (step a). Then Br^- is oxidized rapidly by $[VO(O_2)N_2]$, with creation of Br^+ and $[VO_2N_2]$ at the same time (step b). The oxidized bromides can be used to perform a halogenation reaction when an organic substrate is present (step c). The hydrogen peroxide was decomposed into water and dioxygen in the absence of a substrate (step d) [45]. The catalytic reaction rate would be mainly based on the stability of the formed intermediate $[VO(O_2)N_2]$.

We compared the catalytic activity of some complexes reported previously, and the kinetic data are listed in table 4. It is found that: (i) vanadium(III) complexes show higher catalytic activity than those of vanadium(IV) complexes; (ii) different composition of the vanadium(IV) complexes lead to different rates of formation of the intermediate

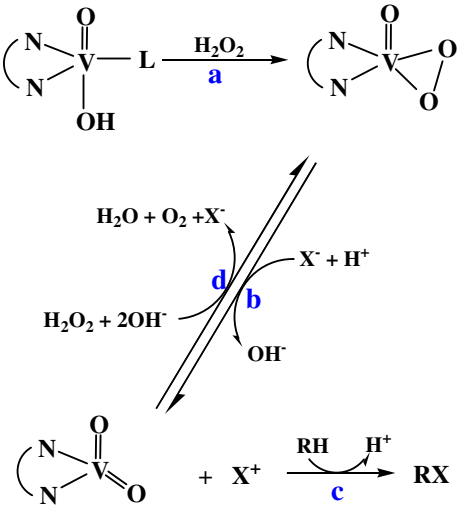

Scheme 4. The catalytic bromination reaction mechanism of the complex.

$[VO(O_2)N_2]$, which can also influence the catalytic activity: (a) the complexes with coordinated H_2O have higher catalytic activity, such as **5**, **6**, and **10**, attributed to low bond energy of the V–O_{H2O} and easy dissociation of water, resulting in easier formation of the intermediate; (b) conjugated tridentate ligand makes the complexes more stable and more difficult to form the intermediate, e.g. **4** and **8**; (c) it is easier for complexes, which contain weakly coordinating ligands, to form the intermediate, such as **11** and **9** (the order of the coordination ability is $C_2O_4^{2-} > SO_4^{2-}$); (d) it is difficult to form the intermediate if the complex has two V=O bonds, such as **1**; (e) different coordination pattern results in a significant

Table 4. Comparisons of the kinetic data for the complexes in DMF–H_2O at 30 ± 0.5 °C.

Complexes	*m*	*b*	$k(M\,L^{-1})^{-2}s^{-1}$	Ref.
1	1.0033	−2.1251	0.187×10^3	This work
2	1.018	−2.1331	0.184×10^3	This work
3[a]	1.0458	−2.1349	0.183×10^3	[34]
4[b]	1.0314	−2.0537	0.221×10^3	[34]
5[c]	1.0381	−1.0857	2.054×10^3	[21]
6[d]	1.0495	−1.3284	1.174×10^3	[21]
7[e]	1.0527	−2.2581	0.14×10^3	[20]
8[f]	1.0976	−2.11	0.19×10^3	[20]
9[g]	1.0666	−1.6809	0.52×10^3	[20]
10[h]	1.0967	−1.2923	1.28×10^3	[20]
11[i]	0.9808	−1.5521	0.70×10^3	[20]

[a]$[VO(Tp)(pzTp)]\cdot 2H_2O$.
[b]$[VO(Tp^{4I})(pz)(SCN)]\cdot 1/2CH_2Cl_2$.
[c]$[V_2(dipic)_2(H_2btec)(H_2O)_4]\cdot 2H_2O$.
[d]$V(dipic)(Hbdc)(H_2O)_2$.
[e]$(VO)_2(bpz^*T\text{-}O)$.
[f]$VO(bpz^*eaT)(SCN)_2$.
[g]$V_2(bpz^*eaT)_2(\mu_2\text{-}C_2O_4)(C_2O_4)_2$.
[h]$[VO(SO_4)(bpz^*P)(H_2O)]\cdot H_2O$.
[i]$VO(SO_4)(bpz^*P\text{-}Me)(H_2O)$.

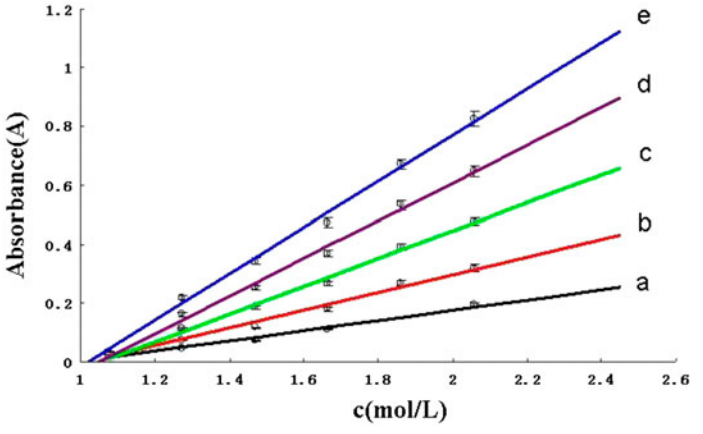

Figure 9. A series of lines of the absorbance at 592 nm dependent on c(H_2O_2) at 5 min intervals of **2** (a: 25 min; b: 30 min; c: 35 min; d: 40 min; e: 45 min). Error bars shown are three standard deviations for three independent measurements.

influence on stability of the complexes, for example, for **1** and **2**, the V–O_{H2bta} bond length of the coordinated 1,2,4,5-benzenetetracarboxylic acid is shorter than that of **6**, indicating formation of the intermediate is more difficult. These results show that the catalytic activity of the complexes may have great connection with their structural characterization.

3.6.3. The effect of the concentration of H_2O_2 on bromination. H_2O_2 is widely used in our daily life and industry [46], and the determination of it is of great practical importance in fields such as foodstuff, clinical physic, pharmaceutical production, and environment protection. So we need a measure to determine H_2O_2 in practical application. We have studied the dependence of the concentration of H_2O_2 and the bromination catalytic reaction to develop a new H_2O_2 detection method. The results show that the oxidation catalyzed by the oxovanadium complexes is H_2O_2 concentration dependent, and the absorbance at 592 nm linearly depends on concentration of H_2O_2 along with the formation of bromophenol blue. A series of lines dependent on c(H_2O_2) at 5 min intervals (among 25–45 min) were plotted for **2** (figure 9). The detection limit of the concentration H_2O_2 was estimated to be 1.0 M L^{-1} by extension of the line. All these observations further confirmed that the catalytic reaction system can be used as a method for H_2O_2 detection, and the complex can be used as a potential diagnostic kit for H_2O_2. In the literature [47], 30–40 min is needed for the complexes to complete the reaction, while we could get good linear relations from 25 to 45 min in this work, perhaps from different structures of the complexes. These experiment results are similar to those of the literature [48].

4. Conclusion

Two vanadium(IV) complexes with 1,2,4,5-benzenetetracarboxylic acid ligands have been synthesized by hydrothermal reaction of $V_2(SO_4)_3$(III) in methanol–water solution, and the single crystal structure data have been obtained. To explore the model oxovanadium

complexes for the active center of VHPO and the further study of the H_2O_2 detection system, bromination activities were tested with phenol red as organic substrate in the presence of H_2O_2, KBr, and phosphate buffer. By comparing with complexes in the literature, the complexes are good candidates for H_2O_2 detection system upon phenol red bromination since the reaction time is shorter. Based on the results, we expect that a fast, simple, and sensitive H_2O_2 detection device will be exploited in the future. Further research of practical application of the H_2O_2 detection is ongoing.

Supplementary material

Tables of atomic coordinates, isotropic thermal parameters, and complete bond distances and angles have been deposited with the Cambridge Crystallographic Data Center. Copies of this information may be obtained free of charge by quoting the publication citation and deposition number CCDC: 952227 for **1**, from the Director, CCDC, 12 Union Road, Cambridge, CB2 1EZ, UK (Fax:+ 44 1223 336033; E-mail: deposit@ccdc.cam.ac.uk or http://www.ccdc.cam.ac.uk).

Funding

This study was supported by the grants of the National Natural Science Foundation of China [grant number 21071071], [grant number 21371086] for financial assistance.

References

[1] C.J. Schneider, J.E. Penner-Hahn, V.L. Pecoraro. *J. Am. Chem. Soc.*, **130**, 2712 (2008).
[2] C. Wikete, P. Wu, G. Zampella, L. De Gioia, G. Licini, D. Rehder. *Inorg. Chem.*, **46**, 196 (2007).
[3] A. Butler. *Coord. Chem. Rev.*, **187**, 17 (1999).
[4] D.C. Crans, L. Yang, J.A. Alfano, L.H. Chi, W. Jin, M. Mahroof-Tahir, K. Robbins, M.M. Toloue, L.K. Chan, A.J. Plante, R.Z. Grayson, G.R. Willsky. *Coord. Chem. Rev.*, **237**, 13 (2003).
[5] K.H. Thompson, J.H. McNeill, C. Orvig. *Chem. Rev.*, **99**, 2561 (1999).
[6] H.B. ten Brink, H.E. Schoemaker, R. Wever. *Eur. J. Biochem.*, **268**, 132 (2001).
[7] T. Moriuchi, M. Yamaguchi, K. Kikushima, T. Hirao. *Tetrahedron Lett.*, **48**, 2667 (2007).
[8] D. Rehder. *J. Inorg. Biochem.*, **102**, 1152 (2008).
[9] J.W.P.M. Vanschijndel, L.H. Simons, E.G.M. Vollenbroek, R. Wever. *FEBS Lett.*, **336**, 239 (1993).
[10] D. Wischang, M. Radlow, J. Hartung. *Dalton Trans.*, 11926 (2013).
[11] D. Wischang, O. Brucher, J. Hartung. *Coord. Chem. Rev.*, **255**, 2204 (2011).
[12] G.J. Colpas, B.J. Hamstra, J.W. Kampf, V.L. Pecoraro. *J. Am. Chem. Soc.*, **118**, 3469 (1996).
[13] M.V. Kirillova, M.L. Kuznetsov, P.M. Reis, J.A.L. Silva, J.J.R.F. Silva, A.J.L. Pombeiro. *J. Am. Chem. Soc.*, **129**, 10531 (2007).
[14] J.N. Carter-Franklin, A. Butler. *J. Am. Chem. Soc.*, **126**, 15060 (2004).
[15] G. Zampella, P. Fantucci, V.L. Pecoraro, L.D. Gioia. *J. Am. Chem. Soc.*, **127**, 953 (2005).
[16] E. Kime-Hunt, K. Spartalian, M. DeRusha, C.M. Nunn, C.J. Carrano. *Inorg. Chem.*, **28**, 4392 (1989).
[17] M. Bagherzadeh, M.M. Haghdoost, A. Shahbazirad. *J. Coord. Chem.*, **65**, 591 (2012).
[18] Y.H. Xing, Z. Sun, W. Zou, J. Song, K. Aoki, M.F. Ge. *J. Struct. Chem.*, **47**, 913 (2006).
[19] Y.H. Xing, K. Aoki, Z. Sun, M.F. Ge, S.Y. Niu. *J. Chem. Res.*, **108**, 2, (2007).
[20] Y.H. Xing, Y.H. Zhang, Z. Sun, L. Ye, Y.T. Xu, M.F. Ge, B.L. Zhang, S.Y. Niu. *J. Inorg. Biochem.*, **101**, 36 (2007).
[21] H.Y. Zhao, Y.H. Xing, Y.Z. Cao, Z.P. Li, D.M. Wei, X.Q. Zeng, M.F. Ge. *J. Mol. Struct.*, **938**, 54 (2009).
[22] Y.Z. Cao, D.M. Wei, D.X. Ren, C. Chen, Y.H. Xing, Z. Shi. *Acta Phys. Chim. Sin.*, **27**, 539 (2011).

[23] C. Chen, Q. Sun, D.X. Ren, R. Zhang, F.Y. Bai, Y.H. Xing, Z. Shi. *CrystEngComm*, **15**, 5561 (2013).
[24] D.X. Ren, N. Xing, H. Shan, C. Chen, Y.Z. Cao, Y.H. Xing. *Dalton Trans.*, 5379 (2013).
[25] G.M. Sheldrick. *SADABS, Program for Empirical Absorption Correction for Area Detector Data*, University of Göttingen, Göttingen (1996).
[26] G.M. Sheldrick. *SHELXS 97, Program for Crystal Structure Refinement*, University of Göttingen, Göttingen (1997).
[27] E. Verhaeghe, D. Buisson, E. Zekri, C. Leblanc, P. Potin, Y. Ambroise. *Anal. Biochem.*, **379**, 60 (2008).
[28] G. Zampella, J.Y. Kravitz, C.E. Webster, P. Fantucci, M.B. Hall, H.A. Carlson, V.L. Pecoraro, L.D. Gioia. *Inorg. Chem.*, **43**, 4127 (2004).
[29] Y.T. Li, C.W. Yan, H.S. Guan. *Polish J. Chem.*, **78**, 1 (2004).
[30] M.K. Chaudhuri, S.K. Chettri, P.C. Paul, P. Srinivas. *J. Fluor. Chem.*, **78**, 131 (1996).
[31] L.J. Wan, C.S. Zhang, Y.H. Xing, Z. Li, N. Xing, L.Y. Wan, H. Shan. *Inorg. Chem.*, **51**, 6517 (2012).
[32] J. Tatiersky, S. Pacigová, M. Sivák, P. Schwendt. *J. Argent. Chem. Soc.*, **97**, 181 (2009).
[33] C. Chen, F.Y. Bai, R. Zhang, G. Song, H. Shan, N. Xing, Y.H. Xing. *J. Coord. Chem.*, **66**, 671 (2013).
[34] Z.P. Li, Y.H. Xing, Y.Z. Cao, X.Q. Zeng, M.F. Ge, S.Y. Niu. *Polyhedron*, **28**, 865 (2009).
[35] C.J. Ballhausen, H.B. Gray. *Inorg. Chem.*, **1**, 111 (1962).
[36] U. Saha, T.K. Si, P.K. Nandi, K.K. Mukherjea. *Inorg. Chem. Commun.*, **38**, 43 (2013).
[37] T.C. Stamatatos, S.P. Perlepes, C.P. Raptopoulou, A. Terzis, N. Klouras. *Inorg. Chim. Acta*, **394**, 747 (2013).
[38] V. Jodaian, M. Mirzaei, M. Arca, M.C. Aragoni, V. Lippolis, E. Tavakoli, N.S. Langeroodi. *Inorg. Chim. Acta*, **400**, 107 (2013).
[39] D. Wischang, M. Radlow, H. Schulz, H. Vilter, L. Viehweger, M.O. Altmeyer, C. Kegler, J. Herrmann, R. Muller, F. Gaillard, L. Delage, C. Leblanc, J. Hartung. *Bioorg. Chem.*, **44**, 25 (2012).
[40] A. Coletti, P. Gallonia, A. Sartorelb, V. Contea, B. Floris. *Catal. Today*, **192**, 44 (2012).
[41] R.I. Rosa, M.J. Clague, A. Butler. *J. Am. Chem. Soc.*, **114**, 760 (1992).
[42] M.R. Maurya, S. Agarwal, C. Bader, M. Ebel, D. Rehder. *Dalton Trans.*, 537 (2005).
[43] M.R. Maurya, A. Kumar, M. Ebel, D. Rehder. *Inorg. Chem.*, **45**, 5924 (2006).
[44] T.N. Mandal, S. Roy, A.K. Barik, S. Gupta, R.J. Butcher, S.K. Kar. *Polyhedron*, **27**, 3267 (2008).
[45] M.J. Clague, A. Butler. *J. Am. Chem. Soc.*, **117**, 3415 (1995).
[46] O. Bortolini, V. Conte, C. Chiappe, G. Fantin, M. Fogagnolo, S. Maietti. *Green Chem.*, **4**, 94 (2002).
[47] R. Zhang, J. Liu, C. Chen, Y.H. Xing, Q.L. Guan, Y.N. Hou, X. Wang, X.X. Zhang, F.Y. Bai. *Spectrochim. Acta, Part A*, **115**, 476 (2013).
[48] S. Liu, J.Q. Tian, L. Wang, Y.W. Zhang, Y.L. Luo, H.Y. Li, A.M. Asiri, A.O. Al-Youbi, X.P. Sun. *ChemPlusChem.*, **77**, 541 (2012).